

Density Functional Study of Calcium Nitride: Refined Geometries and Prediction of High-Pressure Phases

S. Rebecca Römer,[†] Wolfgang Schnick,[†] and Peter Kroll^{*‡}

Department Chemie and Biochemie, Lehrstuhl für Anorganische Festkörperchemie, Ludwig-Maximilians-Universität München, Butenandtstrasse 5-13 (D), D-81377 München, Germany, and Department of Chemistry and Biochemistry, The University of Texas at Arlington, 700 Planetarium Place, Arlington, Texas 76019-0065

Received: August 29, 2008; Revised Manuscript Received: December 2, 2008

The high-pressure behavior of Ca_3N_2 is studied up 100 GPa using density functional theory. Evaluation of many hypothetical polymorphs of composition A_3X_2 leads us to propose four high-pressure polymorphs for both α - and β - Ca_3N_2 : (1) an anti- Rh_2O_3 -II structure at 5 GPa, (2) an anti-B-sesquioxide structure at 10 GPa, (3) an anti-A-sesquioxide structure at 27 GPa, and (4) a hitherto unknown hexagonal structure ($P6_3/mmc$), derived from the post-perovskite structure of CaIrO_3 , at 38 GPa. The development of the density and bulk modulus under pressure has been examined.

I. Introduction

Ca_3N_2 has been known for over 100 years, and its synthesis was reported as early as 1898 by Moissan.¹ It is widely used as a starting material for the synthesis of multinary nitrides or as a flux.² In industry, Ca_3N_2 finds application—among others—as an additive in the refinement process of steel³ and as a catalyst for the transformation of hexagonal BN into cubic BN.⁴

Three different structural modifications of Ca_3N_2 have been discussed in the literature: (1) α - Ca_3N_2 (maroon or yellow, cubic, synthesized at $T > 700$ °C), (2) " β - Ca_3N_2 " (black, hexagonal or tetragonal, synthesized at $T < 700$ °C), and (3) HP/HT- Ca_3N_2 (orthorhombic, synthesized at 1800 °C and 46 kbar).^{5–8} The structure of α - Ca_3N_2 (anti-bixbyite; C-sesquioxide) has been proposed early on.^{8,9} The true nature of " β - Ca_3N_2 " has recently been questioned. It apparently is a Na–Ca–N compound, possibly a Na–Ca subnitride.¹⁰ The description of the HP/HT phase of Ca_3N_2 by Bradley et al.⁷ is, unfortunately, the only reference addressing synthesis and characterization of this modification in the literature. The continuing interest in Ca–N compounds then is manifested in the recent synthesis of a new modification of Ca_3N_2 at 200 and 420 °C from the elements or from Ca_2N and N_2 by Höhn.¹¹ Careful structural characterization revealed a hexagonal (corundum) structure. As a second phase of Ca_3N_2 established beyond doubts, this modification was termed β - Ca_3N_2 .

The relation of α - and β - Ca_3N_2 to the anti-structures of some sesquioxides motivates the search of potential high-pressure phases of Ca_3N_2 among the (anti-)HP-phases of M_2O_3 oxides, which exhibit a very rich high-pressure chemistry. Recent advances in instrumentation and characterization have shown a tremendous amount of new discoveries. For example, Mn_2O_3 , bixbyite, transforms into the post-perovskite structure (CaIrO_3 -type) at 27–38 GPa.¹² Besides the post-perovskite structure type, the Rh_2O_3 -II and the perovskite structure are also widely discussed high-pressure candidates for several sesquioxides. Many binary oxides with a corundum structure at ambient

pressure have been found to undergo phase transformations first into a Rh_2O_3 -II structure, then further at even higher pressures into a perovskite and post-perovskite modification.^{13–26} Corundum (α - Al_2O_3) itself transforms into Rh_2O_3 -II at 80–100 GPa and is predicted to undergo a second phase transformation at 131–156 GPa, which has been recently observed at 130 GPa.^{13–22} The higher homologue In_2O_3 has been predicted to exhibit a transformation from bixbyite to Rh_2O_3 -II at 10 GPa and further to post-perovskite at about 45 GPa.²⁷ Most recent experiments confirm the prediction of the Rh_2O_3 -II phase for both Ga_2O_3 and In_2O_3 .²⁸ Hematite (Fe_2O_3) exhibits both phase transformations, into Rh_2O_3 -II at 50–56 GPa and into post-perovskite at 65 GPa.^{24,26}

These studies and the existence of a not further characterized HP/HT- Ca_3N_2 phase prompted our endeavor to investigate the structural behavior of Ca_3N_2 at high pressures. Naturally, we focused on the aforementioned high-pressure phases of bixbyite and sesquioxides, but did an extensive survey of other potential candidate structures.

II. Method

Structural optimizations, total energies, and properties are calculated within density functional theory (DFT),²⁹ for which we use the Vienna ab initio simulation package (VASP). It combines the total energy pseudopotential method with a plane-wave basis set.^{30–32} The electron exchange and correlation energy is treated within the generalized gradient approximation (GGA).³³ We employ the projector-augmented-wave (PAW) method.³⁴ The cutoff energy for the expansion of the wave function into the plane wave basis is 500 eV. Residual forces are converged below 5×10^{-3} eV/Å. The Brillouin-zone integration is done via the Monkhorst–Pack scheme.³⁵

Structure optimizations are obtained through relaxation of all structural parameters, positions as well as cell parameters. The unit cell of α - Ca_3N_2 contains 80 atoms, corresponding to 16 formula units. We compute this structure using the conventional unit cell and a $2 \times 2 \times 2$ k -point mesh. The unit cell of β - Ca_3N_2 contains 30 atoms (six formula units). A k -point mesh of $6 \times 6 \times 2$ is used for the optimization. The unit cell of γ - Ca_3N_2 (anti- Rh_2O_3 -II structure) comprises 20 atoms, and we use an

* Corresponding author. Phone: (+1)-817-272-3814. Fax: (+1)-817-272-3808. E-mail: pkroll@uta.edu.

[†] Ludwig-Maximilians-Universität München.

[‡] The University of Texas at Arlington.

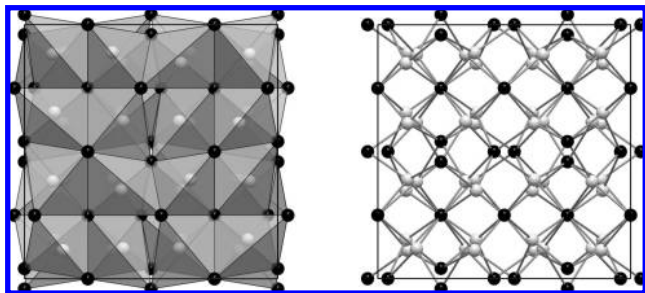


Figure 1. Anti-bixbyite structure of α - Ca_3N_2 —view along $[100]$ (Ca atoms are depicted in light gray, N atoms are black). On the left side, CaN_4 tetrahedra are shown.

$8 \times 8 \times 4$ k -point mesh. For δ - Ca_3N_2 (anti-B-sesquioxide structure; 30 atoms in the unit cell) a $2 \times 4 \times 6$ k -point mesh was employed. The unit cell of ε - Ca_3N_2 (anti-A-sesquioxide structure) contains five atoms, the c/a ratio was fixed at 1.29, and a k -point mesh of $6 \times 6 \times 4$ is used. Finally, for λ - Ca_3N_2 , a new potential high-pressure phase that emerged out of several candidates and is derived from the anti-post-perovskite structure, we employed an $8 \times 8 \times 4$ k -point mesh for the structure which contains 10 atoms 2 formula units). Although we present these relevant structures in detail, we note that we computed a wide selection of about two-dozen candidate structures with composition Ca_3N_2 .

Our choice of the GGA functional is based on the experience that it describes significantly better the relative energies of structures with different coordination of the atoms. Since our target is to study structures and structural transformations at high pressures, it is the better choice in comparison to the local density approximation (LDA). Therefore, although we controlled all our calculations within the LDA as well, all enthalpy differences and transition pressures given in this publication are based on GGA calculations.

To obtain the bulk modulus the volume is varied around the zero-pressure volume V_0 , and the calculated energies are fitted to Murnaghans equation of state (EOS).³⁶ The $E-V$ diagrams are transformed easily to give enthalpy versus pressure diagrams. We extract the pressure p from the $E-V$ graph by numerical differentiation of the equations of state. The enthalpy H is calculated via $H = E + pV$.

In equilibrium a system will adopt the structure with the lowest Gibbs energy G . A phase transformation is therefore governed by the difference of Gibbs energy: $\Delta G = \Delta H - T\Delta S$. The contributions of entropy differences are usually neglected. This is justified, because differences in entropy between extended solid-state structures are small in comparison to changes of ΔH within a few gigapascals of pressure change. Therefore, the enthalpy difference ΔH is a good measure to compare the relative stability of solid-state structures under pressure.

However, if variations from the ideal crystal structure occur, e.g., defects or disorder among atoms, entropic effects may become significant enough to impact the sequence of phases that appear in a phase diagram. We do not treat such terms in our study but will have to take them into account when comparing experimental and computational results.

III. Results

III.a. Optimized Structures. We computed a wide selection of candidate structures with composition Ca_3N_2 . Six polymorphs prove to be relevant for being considered in the phase diagram. α - Ca_3N_2 (Figure 1) adopts an anti-bixbyite structure, space group

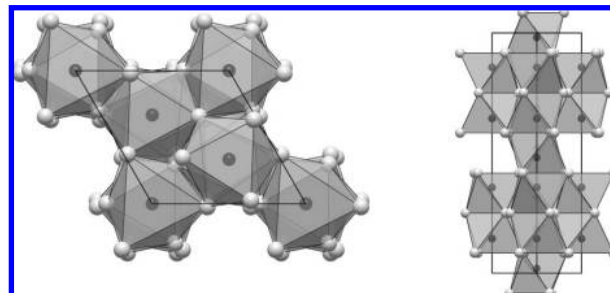


Figure 2. Anticorundum structure of β - Ca_3N_2 (Ca atoms are depicted in light gray, N atoms are black; in both pictures NCa_6 octahedra are drawn; left side, view along $[001]$; right side, view along $[-0.5\ 0.5\ 0]$).

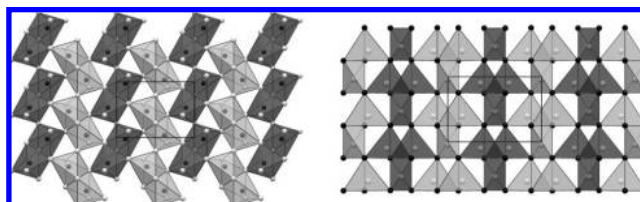


Figure 3. Anti- Rh_2O_3 -II structure of γ - Ca_3N_2 (Ca atoms are depicted in light gray, N atoms are black; left side, NCa_6 octahedra layer viewed along $[001]$; right side, CaN_4 tetrahedra viewed along $[010]$).

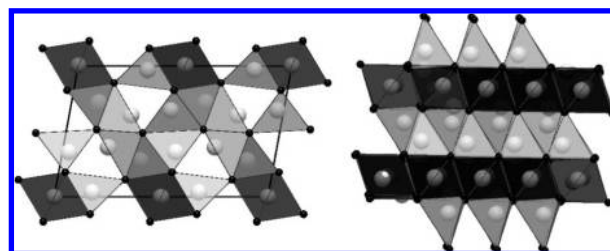


Figure 4. Anti-B-sesquioxide structure of δ - Ca_3N_2 (Ca atoms are depicted in light gray, N atoms are black; left side, view along $[010]$; right side, view along $[\frac{1}{3}\ 1\ \frac{2}{3}]$; note the similarity to Figure 5, right side ε - Ca_3N_2).

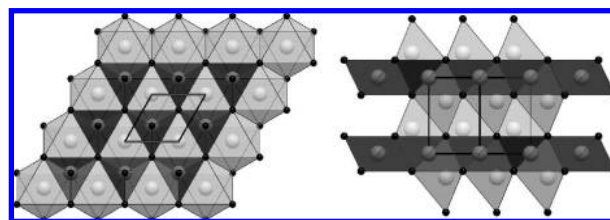


Figure 5. Anti-A-sesquioxide structure of ε - Ca_3N_2 (Ca atoms are depicted in light gray, N atoms are black; left side, view along $[001]$; right side, view along $[\frac{1}{2}\ \frac{1}{2}\ 0]$; note the similarity to Figure 4, right side δ - Ca_3N_2).

$Ia\bar{3}$ (no. 206).³⁷ β - Ca_3N_2 crystallizes in the trigonal space group $R\bar{3}c$ (no. 167) in the anti- Al_2O_3 structure (Figure 2).¹¹ The third candidate structure we find adopts an orthorhombic anti- Rh_2O_3 -II structure, space group $Pbna$ (no. 60) (see Figure 3).²³ Anticipating our results and the discussion, we denote this polymorph as γ - Ca_3N_2 . All these three structures comprise Ca atoms tetrahedrally coordinated by N and N atoms in octahedral coordination by Ca. The fourth structure—denoted δ - Ca_3N_2 —exhibits the monoclinic B-sesquioxide structure (space group $C2/m$, no. 12)³⁸ (Figure 4), and the fifth structure—denoted ε - Ca_3N_2 —exhibits the trigonal A-sesquioxide structure (space group $P\bar{3}m1$, no. 164)³⁹ (Figure 5). In δ - Ca_3N_2 the coordination numbers of Ca and N are partially increased. Whereas in α -, β -, and γ - Ca_3N_2 Ca is always tetrahedrally and N octahedrally

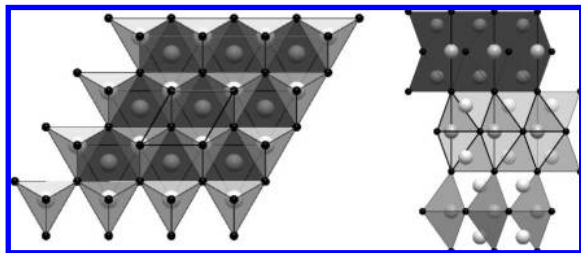


Figure 6. Structure of λ -Ca₃N₂ (Ca atoms are depicted in light gray, N atoms are black; left side, view along [001], CaN₆ octahedra are depicted in black, CaN₅ trigonal bipyramids are light gray; right side, view along [0.5 0.5 0], interpenetrating networks of corner-sharing CaN₅ trigonal bipyramids and double-layers of face-sharing CaN₆ octahedra).

TABLE 1: Computed and Experimental Crystallographic Data of α -Ca₃N₂

		GGA			exptl ^a		
space group		$Ia\bar{3}$ (no. 206)					
Z		16					
a/pm		1145.36			1147.86(2)		
V/10 ⁶ pm ³		1502.55			1512.40		
ρ /g cm ⁻³		2.62			2.60		
atom	Wyc.	x	y	z	x	y	z
Ca1	48e	0.38965	0.15424	0.38269	0.389(1)	0.153(1)	0.382(1)
N1	8b	1/4	1/4	1/4	1/4	1/4	1/4
N2	24d	0.96059	0	1/4	0.960(2)	0	1/4

^a Ref 37.

coordinated (as in Ca₃[⁴N]₂[⁶]), in δ -Ca₃N₂ Ca exhibits a four-, five-, and six-fold coordination (tetrahedrally, quadratic prismatically, octahedrally) and N a six- and seven-fold coordination (octahedrally and seven-fold), the coordination description being [Ca_{2/3}[⁴Ca_{2/9}[⁵Ca_{1/9}[⁶N_{1/3}[⁶N_{2/3}[⁷]]. For ε -Ca₃N₂ coordination numbers are further increased to five (trigonal bipyramids) and six (octahedra) for Ca and eight for N (cubes) (Ca_{2/3}[⁵Ca_{1/3}[⁶N_{3/3}[⁸]). Given the sequence of the antistructures of bixbyite, corundum, and Rh₂O₃-II, yet another high-pressure phase with an (anti-)post-perovskite structure would be rational. But when compressing Ca₃N₂ in the post-perovskite structure (space group *Cmcm*, no. 63),⁴⁰ we found a distortion toward a higher hexagonal symmetry. This sixth candidate structure, termed λ -Ca₃N₂, has been identified with space group *P6₃/mmc* (no. 194) (Figure 6). It exhibits a hitherto undetected structure of Ca₃N₂ which is related to that of β -Be₃N₂ (The Wyckoff positions for M1, M2, and N1 are the same, but N2 occupies the 2d position in λ -Ca₃N₂ and the 2c position in β -Be₃N₂).⁴¹ λ -Ca₃N₂ exhibits partially increased coordination numbers for Ca and N compared to ε -Ca₃N₂. Whereas the coordination polyhedra of Ca remain unchanged, the ratio of CN = 5 to CN = 6 shifts from 2:1 to 1:2. N is now eight- and nine-fold coordinated (Figure 6). For all optimized structures the coordination numbers of the M²⁺ ions were determined by calculating effective coordination numbers (ECoN)⁴² with MAPLE,^{43,44} in order to compare them to the data for the experimentally determined structures (if available). In Tables 1–6 we list the computed crystallographic data of our six polymorphs and compare them with available experimental values. For α -Ca₃N₂ we have also compared them to the results of previous calculations, which are in good accordance with our results.^{45,46}

The calculated bond lengths Ca–N (α -Ca₃N₂, 245–247 pm; β -Ca₃N₂, 241–253 pm; γ -Ca₃N₂, 240–259 pm) are all in the range of those in α -Ca₃N₂ (245–249 pm³⁷) and β -Ca₃N₂ (242–252 pm¹¹) and correspond well to the sum of the ionic

TABLE 2: Computed and Experimental Crystallographic Data of β -Ca₃N₂

		GGA			exptl ^a		
space group		$R\bar{3}c$ (no. 167)					
Z		6					
a/pm		618.48			618.94		
c/pm		1662.13			1661.15		
V/10 ⁶ pm ³		550.61			551.11		
ρ /g cm ⁻³		2.68			2.69		
atom	Wyc.	x	y	z	x	y	z
Ca1	18e	0.30000	0	0.25	0.30005	0	0.25
N1	12c	0	0	0.35349	0	0	0.35254

^a Ref 11.

TABLE 3: Computed Crystallographic Data of γ -Ca₃N₂

		GGA		
space group		<i>Pbcn</i> (no. 60)		
Z		4		
a/pm		620.30		
b/pm		635.20		
c/pm		895.97		
V/10 ⁶ pm ³		353.03		
ρ /g cm ⁻³		2.79		
atom	Wyc.	x	y	z
Ca1	8d	0.60627	0.10513	0.84712
Ca2	4c	0.04498	1/4	0
N1	8d	0.75278	0.03142	0.11210

TABLE 4: Computed Crystallographic Data of δ -Ca₃N₂

		GGA		
space group		<i>C2/m</i> (no. 12)		
Z		6		
a/pm		1504.98		
b/pm		378.30		
c/pm		934.90		
β /deg		100.54		
V/10 ⁶ pm ³		523.30		
ρ /g cm ⁻³		2.82		
atom	Wyc.	x	y	z
Ca1	4i	0.12567	0	0.27775
Ca2	4i	0.32800	1/2	0.03518
Ca3	4i	0.28973	1/2	0.37949
Ca4	4i	0.46826	0	0.33945
Ca5	2b	0	1/2	0
N1	4i	0.14105	1/2	0.48828
N2	4i	0.18256	1/2	0.13023
N3	4i	0.46936	1/2	0.18775

radii (ionic radii after Shannon, $\sum \text{Ca}^{[6]}-\text{N}^{[4]} = 246$ pm;⁴⁷ ionic radii after Baur, $\sum \text{Ca}^{[4]}-\text{N}^{[6]} = 246$ pm; $\sum \text{Ca}^{[6]}-\text{N}^{[8]} = 257$ pm).⁴⁸ For δ -Ca₃N₂, ε -Ca₃N₂, and λ -Ca₃N₂ the dispersion of bond lengths is larger (δ -Ca₃N₂, 233–280 pm; ε -Ca₃N₂, 244–296 pm; λ -Ca₃N₂, 224–330 pm) with the longest Ca–N distances in λ -Ca₃N₂ being found for the two vertices of the CaN₅ trigonal bipyramids, which are substantially reduced under pressure.

III.b. Total Energies, Densities, and Bulk Moduli. Referring to our GGA calculations at ambient pressure, α -Ca₃N₂ has the lowest energy of the four polymorphs (–26.728 eV per formula unit) and also the lowest density, $\rho = 2.62$ g cm⁻³ (exptl value 2.61 g cm⁻³). β -Ca₃N₂ is only about 0.072 eV per formula unit higher in energy, but also about 2.3% denser (computed 2.68 g cm⁻³, matching exptl 2.68 g cm⁻³). The density of γ -Ca₃N₂ ($\rho = 2.79$ g cm⁻³) is higher than that of both α - and

TABLE 5: Computed Crystallographic Data of ϵ -Ca₃N₂

		GGA (<i>c/a</i> = 1.29)			GGA (<i>c/a</i> = 1.78)		
space group		$P\bar{3}m1$ (no. 164)					
<i>Z</i>		1					
<i>a</i> /pm		419.71			385.72		
<i>c</i> /pm		539.83			685.20		
<i>V</i> /10 ⁶ pm ³		82.35			88.29		
ρ /g cm ⁻³		2.99			2.79		
atom	Wyc.	<i>x</i>	<i>y</i>	<i>z</i>	<i>x</i>	<i>y</i>	<i>z</i>
Ca1	2d	1/3	2/3	0.68311	1/3	2/3	0.66459
Ca2	1a	0	0	0	0	0	0
N1	2d	1/3	2/3	0.23052	1/3	2/3	0.23087

TABLE 6: Computed Crystallographic Data of λ -Ca₃N₂

		GGA		
space group		$P6_3/mmc$ (no. 194)		
<i>Z</i>		2		
<i>a</i> /pm		389.11		
<i>c</i> /pm		1318.63		
<i>V</i> /10 ⁶ pm ³		172.90		
ρ /g cm ⁻³		2.85		
atom	Wyc.	<i>x</i>	<i>y</i>	<i>z</i>
Ca1	4f	1/3	2/3	0.08620
Ca2	2b	0	0	1/4
N1	2a	0	0	0
N2	2d	2/3	1/3	1/4

β -Ca₃N₂, about 6.4% and 4.0%, respectively. The energy of γ -Ca₃N₂ in its ground state comes out 0.163 eV per formula unit higher with respect to α -Ca₃N₂. δ -Ca₃N₂ ($\rho = 2.79$ g cm⁻³) is 7.6% denser than α -Ca₃N₂ and 1.1% denser than γ -Ca₃N₂. Its ground-state energy is 0.239 eV above that of α -Ca₃N₂ and 0.077 eV above that of γ -Ca₃N₂. ϵ -Ca₃N₂ then is the polymorph with the highest density we found. With $\rho = 2.99$ g cm⁻³ it is about 14.1% denser than α -Ca₃N₂, 7.2% denser than γ -Ca₃N₂, and 5.7% denser than δ -Ca₃N₂. Its energy lays 0.850 eV above that of α -Ca₃N₂ and 0.611 eV above that of δ -Ca₃N₂. Finally, λ -Ca₃N₂ is lower in density than ϵ -Ca₃N₂ by 4.7%, but it is 8.6% denser than α -Ca₃N₂ and still 2.1% denser than γ -Ca₃N₂ and 1.1% denser than δ -Ca₃N₂. The energy of λ -Ca₃N₂ is 0.980 eV per formula units higher than that of α -Ca₃N₂ and 0.130 eV per formula units higher than that of ϵ -Ca₃N₂. The bulk moduli at ambient pressure of the first three phases increase with increasing density from 68 GPa over 72 to 73 GPa in the sequence of α -, β -, and γ -Ca₃N₂. δ -Ca₃N₂ exhibits an equilibrium bulk modulus B_0 of 67 GPa, ϵ -Ca₃N₂ of 76 GPa, and λ -Ca₃N₂ of 45 GPa.

III.c. $E-V$ Calculations and Resulting $\Delta H-p$ Diagram.

In Figure 7 we show the $E-V$ curves of our six structures of Ca₃N₂. We converted the $E-V$ data into the enthalpy–pressure phase diagram shown in Figure 8 by standard methods.

With respect to enthalpy, it turns out that α -Ca₃N₂ is the most stable polymorph of Ca₃N₂ for pressures up to 5 GPa, at which it will transform to γ -Ca₃N₂. β -Ca₃N₂, on the other hand, does not appear as a valid high-pressure phase from our calculations, which refer to 0 K temperature. Its appearance, we suggest, is likely due to entropy effects that impact the Gibbs energy ΔG at higher temperatures. Once γ -Ca₃N₂ is formed, it will remain stable up to about 10 GPa. At this pressure the monoclinic structure of δ -Ca₃N₂ becomes the most stable polymorph of Ca₃N₂. When pressures exceeding 27 GPa are reached, hexagonal ϵ -Ca₃N₂ is lower in enthalpy and will consequently form. Above 38 GPa, λ -Ca₃N₂ becomes lower in enthalpy.

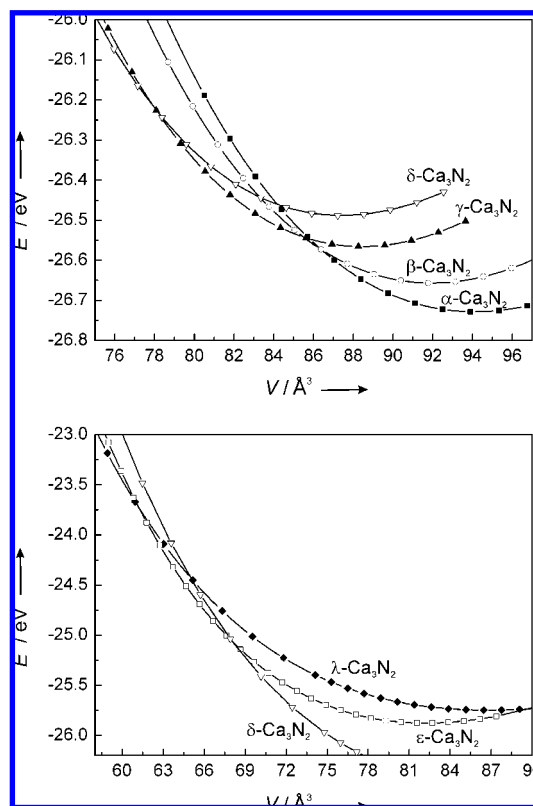


Figure 7. $E-V$ diagrams for six phases of Ca₃N₂: (top) α -Ca₃N₂, β -Ca₃N₂, γ -Ca₃N₂, δ -Ca₃N₂; (bottom) (continuation of top, α -, β -, and γ -phases omitted for clarity) δ -Ca₃N₂, ϵ -Ca₃N₂, λ -Ca₃N₂. The line is a fit to the data according to Murnaghan's EOS.

In total, we thus propose four new high-pressure phases of Ca₃N₂. The sequence of structures together with transition pressures and density increases are illustrated in Figure 9.

IV. Discussion

We succeeded in identifying several promising candidates for high-pressure phases of Ca₃N₂. According to our calculations, γ -Ca₃N₂ is the thermodynamical stable modification between 5 and 10 GPa. Above 10 GPa, another high-pressure phase— δ -Ca₃N₂—becomes lower in enthalpy than γ -Ca₃N₂, easily accessible in today's high-pressure experimental setups. γ -Ca₃N₂ remains thermodynamical stable up to 27 GPa, when ϵ -Ca₃N₂ comes into existence, finally followed by λ -Ca₃N₂ above 38 GPa. The complete pressure range is attainable in diamond anvil cell (DAC) experiments, and the search for high-pressure phases of Ca₃N₂ should provide a fertile soil for discoveries.

About 50 years ago, a high-pressure phase of Ca₃N₂ with orthorhombic structure has been mentioned by Bradley et al.⁷ It was synthesized at 4.6 GPa (and 1800 °C), which matches the transition pressure we computed for α -Ca₃N₂ into γ -Ca₃N₂ very closely. The cell parameters reported at that time, however, do not agree with the data we propose for γ -Ca₃N₂. Nevertheless, this concurrence strongly motivates experiments designated to elucidate the high-pressure behavior of Ca₃N₂.

Although the transition of α -Ca₃N₂ into γ -Ca₃N₂ does not affect the coordination of Ca and N, coordination numbers are successively increased during transforming into δ -, ϵ -, and λ -Ca₃N₂. The average coordination number for Ca increases from 4 (α -, β -, γ -Ca₃N₂) to 4.44 (δ -Ca₃N₂) to 5.33 (ϵ -Ca₃N₂) to 5.67 (λ -Ca₃N₂). The average coordination number for N increases from 6 (α -, β -, γ -Ca₃N₂) to 6.67 (δ -Ca₃N₂) to 8 (ϵ -Ca₃N₂) to 8.67 (λ -Ca₃N₂).

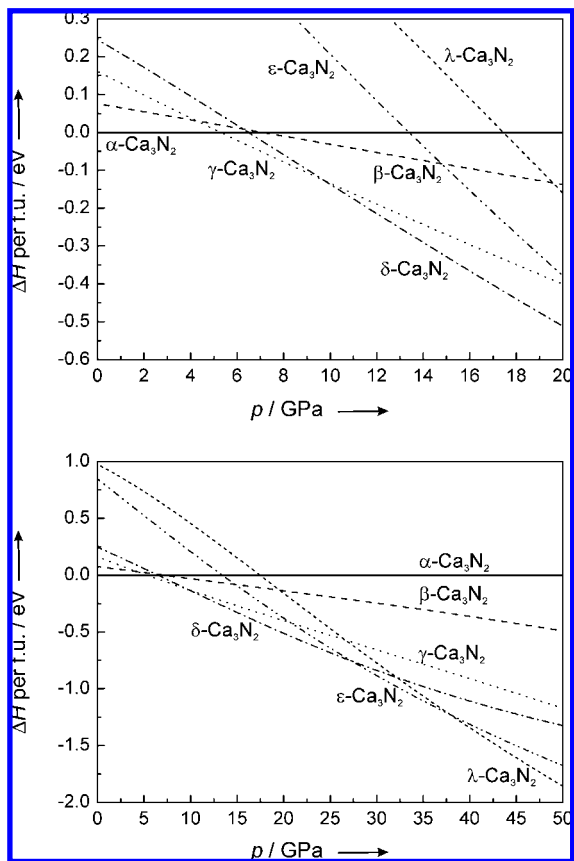


Figure 8. Enthalpy–pressure diagrams for the transition of $\alpha\text{-Ca}_3\text{N}_2$ into $\beta\text{-Ca}_3\text{N}_2$ ($p_t = 6.5$ GPa), $\gamma\text{-Ca}_3\text{N}_2$ ($p_t = 5.0$ GPa), $\delta\text{-Ca}_3\text{N}_2$ ($p_t = 10$ GPa), $\epsilon\text{-Ca}_3\text{N}_2$ ($p_t = 27$ GPa), and $\lambda\text{-Ca}_3\text{N}_2$ ($p_t = 38$ GPa): (top) zoom-in on the transitions of $\alpha\text{-Ca}_3\text{N}_2$ into $\gamma\text{-Ca}_3\text{N}_2$ and $\gamma\text{-Ca}_3\text{N}_2$ into $\delta\text{-Ca}_3\text{N}_2$.

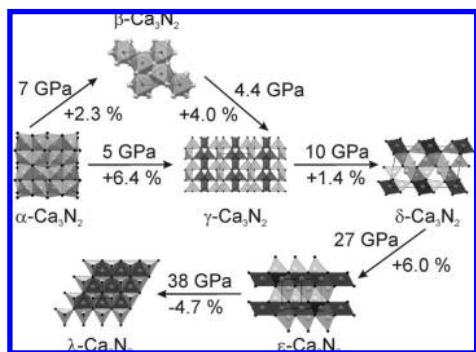


Figure 9. Sequence of structures of Ca_3N_2 together with transition pressures and changes in density.

A constant increase in density is attained by every phase transition up to $\epsilon\text{-Ca}_3\text{N}_2$. Remarkably, $\lambda\text{-Ca}_3\text{N}_2$ is lower in density than $\epsilon\text{-Ca}_3\text{N}_2$ at ambient pressure, although $\lambda\text{-Ca}_3\text{N}_2$ succeeds the ϵ -phase at higher pressure. Although this finding is counterintuitive—one expects a high-pressure phase to be denser than a phase adopted at lower pressure—the reason is based in a very different behavior of density under pressure: $\lambda\text{-Ca}_3\text{N}_2$ simply becomes denser than $\epsilon\text{-Ca}_3\text{N}_2$ above 11 GPa (Figure 10).

The structural developments are somewhat complicated by a strong response of the c/a ratio in $\epsilon\text{-Ca}_3\text{N}_2$ to the applied pressure. Note that above 12 GPa $\epsilon\text{-Ca}_3\text{N}_2$ with a c/a ratio of 1.29 is more favorable (corresponding to an anti- Ni_2Al_3 -type structure³⁹), whereas below 12 GPa the structure suddenly expands to a c/a ratio of 1.78 (denoted ϵ' and corresponding to

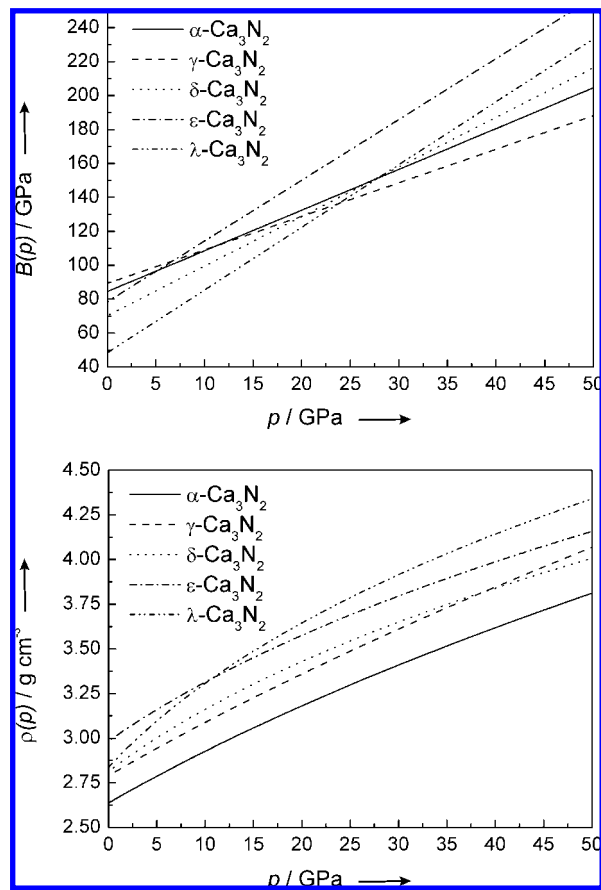


Figure 10. Pressure dependency of the bulk modulus B (top) and the density ρ (bottom) of the high-pressure phases of Ca_3N_2 .

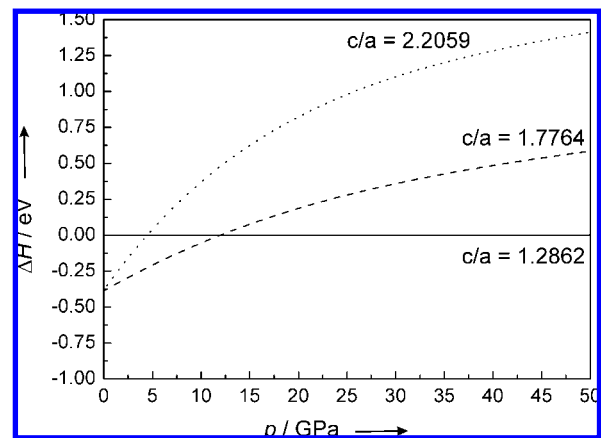


Figure 11. Enthalpy–pressure diagram of $\epsilon\text{-Ca}_3\text{N}_2$ for different fixed c/a ratios.

an anti- La_2O_3 -type structure,³⁹ see Table 5). Computations with fixed ratio c/a clearly indicated the crossover within this (anti)-A-sesquioxide structure type (Figure 11).

When the zero-pressure bulk moduli of the different phases are compared, we see that B_0 increases from 68 to 73 GPa along the sequence α -, β -, and $\gamma\text{-Ca}_3\text{N}_2$ (Table 7). It then decreases to 67 GPa for $\delta\text{-Ca}_3\text{N}_2$, increases to 76 GPa for $\epsilon\text{-Ca}_3\text{N}_2$, and finally, drops to 45 GPa for $\lambda\text{-Ca}_3\text{N}_2$. Note that B_0 of $\epsilon\text{-Ca}_3\text{N}_2$ turns out even lower than that of $\alpha\text{-Ca}_3\text{N}_2$ (68 GPa). Consequently, $\lambda\text{-Ca}_3\text{N}_2$ should be the most compressible and $\epsilon\text{-Ca}_3\text{N}_2$ the least compressible of all discussed modifications of Ca_3N_2 . This also reflects the fact that $\lambda\text{-Ca}_3\text{N}_2$ becomes denser under pressure than $\epsilon\text{-Ca}_3\text{N}_2$, since it is more compressible, and

TABLE 7: E_0 , V_0 , B_0 , ρ , and Band Gap for α -, β -, γ -, δ -, ϵ -, and λ - Ca_3N_2

	E_0 per f.u./eV	V_0 per f.u./ 10^6 pm^3	B_0 / GPa	ρ /g cm^{-3}	band gap/ eV (GGA)	band gap/ eV (LDA)
α - Ca_3N_2	-26.728	93.91	68	2.62	1.16	1.25
β - Ca_3N_2	-26.657	91.77	72	2.68	0.81	0.91
γ - Ca_3N_2	-26.566	88.26	73	2.79	1.36	1.53
δ - Ca_3N_2	-26.489	87.22	67	2.82	1.42	1.65
ϵ - Ca_3N_2	-25.878	82.35	76	2.99	0.99	—
λ - Ca_3N_2	-25.748	86.46	45	2.85	1.46	1.78

therefore the same change in pressure Δp results in a larger volume change ΔV in λ - Ca_3N_2 than in ϵ - Ca_3N_2 .

The development of the bulk moduli under pressure for all considered high-pressure polymorphs is shown in Figure 10.

All high-pressure transitions of Ca_3N_2 should be easily detectable via X-ray diffraction experiments (ex situ and in situ), as the powder patterns of all phases are quite different. Simulated powder patterns for all compounds at the respective transition pressures can be found in the Supporting Information.

In our calculations, β - Ca_3N_2 does not appear as a valid high-pressure phase of Ca_3N_2 , since it is always found to be higher in enthalpy than either α -, γ -, δ -, ϵ -, or λ - Ca_3N_2 . The transition pressure of α - Ca_3N_2 into β - Ca_3N_2 is calculated to 7 GPa and, therefore, higher than the transition pressure of α - Ca_3N_2 into γ - Ca_3N_2 (5 GPa). Moreover, it is higher than the transition pressure of β - Ca_3N_2 into γ - Ca_3N_2 (4.4 GPa). Why can β - Ca_3N_2 then be synthesized at all? Its existence may well be attributed to temperature effects and the influence of entropy on the Gibbs energy. Although entropy differences may have several sources, the amount of defects occurring in β - Ca_3N_2 are expected to dominate over differences in vibrational entropy.¹¹ For crystals containing point defects, the equation for the Gibbs energy $G = H - TS$ has to be rewritten to $G = H_0 - TS_0 + n_D(H_D^f - TS_D^f) - kT(\ln W_D)$, where $H_0 - TS_0$ denotes the Gibbs energy of the perfect crystal, n_D is the number of defects, H_D^f is the enthalpy of defect formation, S_D^f is the thermal entropy, and $kT(\ln W_D)$ is the configurational entropy. These additional terms to the Gibbs energy are not negligible for solids containing a significant defect concentration. Given the small enthalpy difference between α - and β - Ca_3N_2 they may have a substantial influence on the Gibbs energy and, thus, on the phase development.

V. Conclusion

We investigated a manifold of possible structures of high-pressure phases of calcium nitride, Ca_3N_2 , to elucidate the pressure-dependent phase diagram of Ca_3N_2 . Four candidate structures, anti-Rh₂O₃-II (γ - Ca_3N_2), anti-B-sesquioxide (δ - Ca_3N_2), anti-C-sesquioxide (ϵ - Ca_3N_2), and a hitherto undetected hexagonal structure type (λ - Ca_3N_2) are found to become lower in enthalpy under pressure than α - Ca_3N_2 . Although α -, β -, and γ - Ca_3N_2 exhibit the same coordination numbers for Ca and N, the coordination numbers increase toward δ -, ϵ -, and λ - Ca_3N_2 . α - Ca_3N_2 will first transform into γ - Ca_3N_2 at 5 GPa, which in turn transforms into δ - Ca_3N_2 at 10 GPa. At 27 GPa ϵ - Ca_3N_2 becomes the most stable polymorph of Ca_3N_2 , surpassed above 39 GPa by λ - Ca_3N_2 . This very rich high-pressure chemistry of Ca_3N_2 we propose indeed will motivate detailed experiments.

Acknowledgment. Information on β - Ca_3N_2 provided by Dr. P. Höhn, Max-Planck-Institut für Chemische Physik fester Stoffe, Dresden, is gratefully appreciated. Financial support by the Deutsche Forschungsgemeinschaft (priority program SPP 1236, projects SCHN 377/13 and KR 1805/10 and Heisenberg

program Kr 1805/9) as well as the Fonds der Chemischen Industrie (FCI), Germany, is gratefully acknowledged. The authors further thank the Leibniz Rechenzentrum, Munich for computational resources on the Linux Cluster System, as well as the Texas Advanced Computing Center at Austin.

Supporting Information Available: Simulated X-ray powder patterns of the different calculated polymorphs of Ca_3N_2 at the respective transition pressures. This material is available free of charge via the Internet at <http://pubs.acs.org>.

References and Notes

- (1) Moissan, H. C. R. *Hebdomadae Acad. Sci.* **1898**, *127*, 497–501.
- (2) For example: (a) Jian, J. K.; Wang, G.; Wang, C.; Yuan, W. X.; Chen, X. L. *J. Cryst. Growth* **2006**, *291*, 72–76. (b) Hampshire, S.; Park, H. K.; Thompson, D. P.; Jack, K. H. *Nature* **1978**, *274*, 880–882. (c) Vennos, D. A.; Badding, M. E.; DiSalvo, F. J. *Inorg. Chem.* **1990**, *29*, 4059–4062. (d) Chern, Y. M.; Vennos, D. A.; DiSalvo, F. J. *J. Solid State Chem.* **1992**, *96*, 415–425. (e) Schnick, W.; Schultz-Coulon, V. *Angew. Chem.* **1993**, *105*, 308–309; *Angew. Chem., Int. Ed. Engl.* **1993**, *32*, 280–281. (f) Schultz-Coulon, V.; Schnick, W. *Z. Naturforsch., B: Chem. Sci.* **1995**, *50*, 619–622. (g) Rohrer, F. E.; Nesper, R. J. *Solid State Chem.* **1998**, *135*, 194–200. (h) Henry, P. F.; Weller, M. T. *Angew. Chem.* **1998**, *110*, 3040–3041; *Angew. Chem., Int. Ed.* **1998**, *37*, 2855–2857.
- (3) (a) Willners, H. Improving the Quality of Steel. Svensk Patentdnning SE 115621 19460108, 1946. (b) Desulfurizing and Dephosphorizing Agents for Steel and Cast Iron. Jpn. Kokao Tokkyo Koho JP 55094432 19800717, 1980. (c) Kobayashi, H. Refining of Molten Steel. Jpn. Kokai Tokkyo Koho JP 03006314, A, 1991.
- (4) For example: (a) Yin, I.-W.; Li, M.-S.; Liu, Y.-X.; Xu, B.; Sui, J.-L.; Qi, Y.-X. *Adv. Mater.* **2003**, *15*, 720–723. (b) Bocquillon, G.; Loriers-Susse, C.; Loriers, J. J. *Mater. Sci.* **1993**, *28*, 3547–3456.
- (5) Franck, H. H.; Beredig, M. A.; Hoffmann, G. *Naturwissenschaften* **1933**, *21*, 330–331.
- (6) Hartmann, H.; Fröhlich, H. J. *Z. Anorg. Allg. Chem.* **1934**, *218*, 190–192.
- (7) Bradley, R. S.; Munro, D. C.; Whitfield, M. J. *Inorg. Nucl. Chem.* **1966**, *28*, 1803–1812.
- (8) Stackelberg, M. v.; Paulus, R. *Z. Phys. Chem.* **1933**, *22* (B), 365–322.
- (9) Laurent, Y.; Lang, J.; Le Bihan, M. T. *Acta Crystallogr., Sect. B* **1968**, *24*, 494–499.
- (10) Reckeweg, O.; DiSalvo, F. J. *Z. Anorg. Allg. Chem.* **2001**, *627*, 371–377.
- (11) Höhn, P. *Chem. Eur. J.*, submitted for publication, 2008.
- (12) Santillan, J.; Shim, S.-H.; Shen, G.; Prakapenka, V. B. *Geophys. Res. Lett.* **2006**, *33*, L15307/1–L15307/5.
- (13) Tsuchiya, J.; Tsuchiya, T.; Wentzcovitch, R. M. *Phys. Rev. B* **2005**, *72*, 020103/1–020103/4.
- (14) Duan, W.; Wentzcovitch, R. M.; Thomson, K. T. *Phys. Rev. B* **1998**, *57*, 10363–10369.
- (15) Lin, J.-F.; Degtyareva, O.; Prewitt, C. T.; Dera, P.; Sata, N.; Gregoryanz, E.; Mao, H.-K.; Hemley, R. J. *Nat. Mater.* **2004**, *3*, 389–392.
- (16) Funamori, N.; Jeanloz, R. *Science* **1997**, *278*, 1109–1111.
- (17) Mashimo, T.; Tsumoto, K.; Nakamura, K.; Noguchi, Y.; Fukuoka, K.; Syono, Y. *Geophys. Res. Lett.* **2000**, *27*, 2021–2024.
- (18) Cynn, H.; Isaak, D. G.; Cohen, R. E.; Nicol, M. F.; Anderson, O. L. *Am. Mineral.* **1990**, *75*, 439–442.
- (19) Morton, F. C.; Cohen, R. E. *Am. Mineral.* **1994**, *79*, 789–792.
- (20) Thomson, K. T.; Wentzcovitch, R. M.; Bukowinski, M. S. T. *Science* **1996**, *274*, 1880–1882.
- (21) (a) Oganov, A. R.; Ono, S. *Proc. Natl. Acad. Sci. U.S.A.* **2005**, *102*, 10828–10831. (b) Ono, S.; Oganov, A. R.; Koyama, T.; Shimizu, H. *Earth Planet. Sci. Lett.* **2006**, *246*, 326–335.
- (22) Caracas, R.; Cohen, R. E. *Phys. Rev. B* **2007**, *76*, 184104/1–184104/8.
- (23) Shannon, R. D.; Prewitt, C. T. *J. Solid State Chem.* **1970**, *2*, 134–136.
- (24) Rozenberg, Kh. G.; Dubrovinsky, L. S.; Pasternak, M. P.; Naaman, O.; Le Bihan, T.; Ahuja, R. *Phys. Rev. B* **2002**, *65*, 064112/1–064112/8.
- (25) Shim, S.-H.; Duffy, T. S. *Am. Mineral.* **2002**, *87*, 318–326.
- (26) Ono, S.; Ohishi, Y. *J. Phys. Chem. Solids* **2005**, *66*, 1714–1720.
- (27) (a) Gurlo, A.; Kroll, P.; Riedel, R. *Chem. Eur. J.* **2008**, *14*, 3306–3310. (b) Caracas, R.; Cohen, R. E. *Phys. Rev. B* **2007**, *76*, 184101/1–184101/8.
- (28) (a) Yusa, H.; Tsuchiya, T.; Sata, N.; Ohishi, Y. *Phys. Rev. B* **2008**, *77*, 064107/1–9. (b) Gurlo, A.; Dzivenko, D.; Kroll, P.; Riedel, R. *Phys. Status Solidi RRL* **2008**, *2*, 269–271.
- (29) Hohenberg, P.; Kohn, W. *Phys. Rev. B* **1964**, *136*, 864–871.

- (30) Kresse, G. *Phys. Rev. B* **1993**, *47*, 558–561; **1994**, *49*, 14251–14269.
- (31) Kresse, G.; Furthmüller, J. *Comput. Mater. Sci.* **1996**, *6*, 15–50.
- (32) Kresse, G.; Furthmüller, J. *Phys. Rev. B* **1996**, *54*, 11169–11186.
- (33) Perdew, J. P. In *Electronic Structures of Solids '91*; Ziesche, P., Eschrig, H., Eds.; Akademie Verlag: Berlin, 1991.
- (34) Kresse, G.; Joubert, J. *Phys. Rev. B* **1999**, *59*, 1758–1775.
- (35) Monkhorst, H. J.; Pack, J. D. *Phys. Rev. B* **1976**, *13*, 5188–5192.
- (36) Murnaghan, F. D. *Proc. Natl. Acad. Sci. U.S.A.* **1944**, *30*, 244–247.
- (37) Laurent, Y.; Lang, J.; LeBihan, M. Th. *Acta Crystallogr., Sect. B* **1968**, *24*, 494–499.
- (38) Cromer, D. T. *J. Phys. Chem.* **1957**, *61*, 753–755.
- (39) (a) La₂O₃; Barbezat, S.; Lories, J. C. R. *Hebd. Seances Acad. Sci.* **1952**, *234*, 1978–1980. (b) Ni₂Al₃; Bradley, A. J.; Taylor, A. *Philos. Mag.* **1937**, *23*, 1049–1067.
- (40) Rodi, F.; Babel, D. *Z. Anorg. Allg. Chem.* **1965**, *336*, 17–23.
- (41) (a) Eckerlin, P.; Rabenau, A. *Z. Anorg. Allg. Chem.* **1960**, *304*, 218–229. (b) Hall, D.; Gurr, G. E.; Jeffrey, G. A. *Z. Anorg. Allg. Chem.* **1969**, *369*, 108–112.
- (42) Hoppe, R. *Angew. Chem.* **1970**, *82*, 7–16; *Angew. Chem., Int. Ed. Engl.* **1970**, *9*, 25–34.
- (43) (a) Hoppe, R. *Angew. Chem.* **1966**, *78*, 52–63; *Angew. Chem., Int. Ed. Engl.* **1966**, *5*, 95–106. (b) Hoppe, R. *Z. Naturforsch., A: Phys. Sci.* **1995**, *50*, 555–567. (c) Weiss, C.; Hoppe, R. *Z. Anorg. Allg. Chem.* **1996**, *622*, 1019–1026.
- (44) Hübenthal, R. MAPLE, Madlung Part of Lattice Energy (Program), version 4; University of Giessen: Giessen, Germany, 1993.
- (45) Mokhtari, A.; Akbarzadeh, H. *Physica B* **2003**, *337*, 122–129.
- (46) Orhan, E.; Jobic, S.; Brec, R.; Marchand, R.; Saillard, J.-Y. *J. Mater. Chem.* **2002**, *12*, 2475–2479.
- (47) Shannon, R. D. *Acta Crystallogr., Sect. A* **1976**, *32*, 751–767.
- (48) Baur, W. H. *Crystallogr. Rev.* **1987**, *1*, 59–83.

JP8077002